# Systemic characterization of pppGpp, ppGpp and pGpp targets in *Bacillus* reveal SatA converts (p)ppGpp to pGpp to regulate alarmone composition and signaling

Jin Yang[1], Brent W. Anderson[1], Asan Turdiev[2], Husan Turdiev[2], David M. Stevenson[1], Daniel Amador-Noguez[1], Vincent T. Lee[2,*], Jue D. Wang[1,*]

[1] Department of Bacteriology, University of Wisconsin, Madison, WI 53706, USA

[2] Department of Cell Biology and Molecular Genetics, University of Maryland, College Park, Maryland, USA

*Correspondence: wang@bact.wisc.edu; vtlee@umd.edu

**Abstract**

The alarmones pppGpp and ppGpp (collectively (p)ppGpp) protect bacterial cells from nutritional and other stresses. Here we demonstrate the physiological presence of pGpp as a third closely related alarmone in bacterial cells and also characterize and compare the proteomic targets of pGpp, ppGpp and pppGpp in Gram-positive *Bacillus* species. We revealed two regulatory pathways for ppGpp and pppGpp that are highly conserved across bacterial species: inhibition of purine nucleotide biosynthesis and control of ribosome assembly/activity through GTPases. Strikingly, pGpp potently regulates the purine biosynthesis pathway but does not interact with the GTPases. Importantly, we identified a key enzyme SatA that efficiently produces pGpp by hydrolyzing (p)ppGpp, thus tuning alarmone composition to uncouple the regulatory modules of the alarmones. Correspondingly, a *satA* mutant displays significantly reduced pGpp levels and elevated (p)ppGpp levels, slower growth recovery from nutrient downshift, and significant loss of competitive fitness. These cellular consequences for regulating alarmone composition strongly implicate an expanded repertoire of alarmones in a new strategy of stress response in *Bacillus* and its relatives.

18 **Introduction**

19 Organisms from bacteria to humans rely on timely and flexible responses to
20 survive various environmental challenges. The stress signaling nucleotides guanosine
21 tetraphosphate (ppGpp) and guanosine pentaphosphate (pppGpp) are conserved across
22 bacterial species. When induced upon starvation and other stresses, they mediate
23 multiple regulations and pathogenesis by dramatically remodeling the transcriptome,
24 proteome and metabolome of bacteria in a rapid and consistent manner[1–3]. (p)ppGpp
25 interacts with diverse targets including RNA polymerases in *Escherichia coli* [4–6],
26 replication enzyme primase in *Bacillus subtilis*[7–9], purine nucleotide biosynthesis
27 enzymes[10–13], and GTPases involved in ribosome assembly[14–17]. Identification of
28 (p)ppGpp binding targets on a proteome-wide scale is one way to unravel a more
29 extensive interaction network[13,16,18]. However, because binding targets differ between
30 different species and most interactomes have not been characterized, the conserved
31 and diversifying features of these interactomes remain incompletely understood.

32 Another poorly understood aspect of (p)ppGpp is that ppGpp and pppGpp are
33 commonly referred to and characterized as a single species despite potential differences
34 in specificity between the two alarmones[19]. There is evidence for potential existence of a
35 third alarmone, guanosine-5′-monophosphate-3′-diphosphate (pGpp), since several
36 small alarmone synthetases can synthesize pGpp *in vitro*[20,21]. However, pGpp has not
37 been detected in bacterial cells.

38 Here we demonstrate pGpp as a third alarmone in Gram-positive bacteria by
39 establishing its presence in cells, profiling its targets, and identifying a key enzyme for
40 pGpp production through hydrolyzing (p)ppGpp. We also compare the targets of pGpp,
41 ppGpp and pppGpp through proteomic screens in *Bacillus anthracis*. We found that both
42 pppGpp and ppGpp regulate two major cellular pathways: purine synthesis and

43 ribosome biogenesis. In contrast, pGpp strongly regulates purine synthesis targets but
44 does not regulate ribosome biogenesis targets, indicating a separation of regulatory
45 function for these alarmones. In *B. subtilis* and *B. anthracis*, pGpp is efficiently produced
46 from pppGpp and ppGpp by the NuDiX (Nucleoside Diphosphate linked to any moiety
47 "X") hydrolase SatA (Small alarmone (guanosine) triphosphate synthase A), both *in vitro*
48 and *in vivo*. A Δ*satA* mutant has significantly stronger accumulation of pppGpp and
49 decreased accumulation of pGpp, slower recovery from stationary phase and reduced
50 fitness. Our work suggests a mechanism for the conversion and fine tuning of alarmone
51 regulation and the physiological production of the alarmone pGpp.

52

53 **Results**

54 **Proteome-wide screen for binding targets of pppGpp and ppGpp from *Bacillus***
55 ***anthracis***

56 To systematically characterize the binding targets of (p)ppGpp and identify novel
57 (p)ppGpp binding proteins in *Bacillus* species, we screened an open reading frame
58 (ORF) library of 5341 ORFs from the pathogen *Bacillus anthracis* (**Figure 1a**). Using
59 Gateway cloning, we placed each ORF into two expression constructs, one expressing
60 the ORF with an N-terminal histidine (His) tag and the other with an N-terminal histidine
61 maltose binding protein (HisMBP) tag. Each ORF in the His-tagged and HisMBP-tagged
62 library was overexpressed and binding to [5′-α-$^{32}$P]-ppGpp was assayed using
63 differential radial capillary action of ligand assay (DRaCALA)[22] (**Figure 1a**). The fraction
64 of ligand bound to protein in each lysate was normalized as a Z-score of each plate to
65 reduce the influence of plate-to-plate variation (Table S1). We found that the strongest
66 ppGpp-binding targets in *B. anthracis* can be categorized to three groups: 1) purine

67 nucleotide synthesis proteins (Hpt-1, Xpt, Gmk, GuaC, PurA, PurR); 2) ribosome and
68 translation regulatory GTPases (HflX, Der, Obg, RbgA, TrmE, Era); and 3) nucleotide
69 hydrolytic enzymes, including NuDiX hydrolases and nucleotidases (**Figure 1b**).

70 We compared these targets to those obtained from previous screens for ppGpp
71 targets in *E. coli* and for an unseparated mix of (p)ppGpp in *S. aureus* [16]. Comparison of
72 our results with these previous screens yielded conserved themes (**Figure 1b**). Among
73 the most conserved themes are the purine nucleotide synthesis proteins **(Figure 1c)** and
74 ribosome and translation regulation GTPases **(Figure 1d)**.

75 To date, the pppGpp interactome has not been systematically characterized in
76 bacteria. Therefore we performed a separate screen to characterize the binding of the *B.*
77 *anthracis* proteome to [5′-α-$^{32}$P]-pppGpp (**Figure 1a**). We found that pppGpp shares
78 almost identical targets with ppGpp, with similar or reduced binding efficacy for most of
79 its targets compared to ppGpp (**Table S1**). pppGpp is the predominant alarmone
80 induced upon amino acid starvation in *Bacillus* species, and by sharing targets with
81 ppGpp, pppGpp also comprehensively regulates purine synthesis and ribosome
82 assembly. We also find that several proteins bind to pppGpp but not ppGpp, including
83 the small alarmone synthetase YjbM (SAS1). This is expected for YjbM, since it is
84 allosterically activated by pppGpp, but not ppGpp[23].

85

86 **SatA, a NuDiX hydrolase in the (p)ppGpp interactome in *Bacillus*, hydrolyzes**
87 **(p)ppGpp to produce pGpp *in vitro***

88 The putative NuDiX hydrolase, BA5385, was identified as a novel binding target
89 of (p)ppGpp. Protein sequence alignment showed that BA5385 has homologs in different
90 *Bacillus* species with extensive homology and a highly conserved NuDiX box (**Figure**

91 **S1**). We cloned its homolog, YvcI, from the related species *Bacillus subtilis* and showed
92 that overexpressed *B. subtilis* YvcI in cell lysate also binds ppGpp and pppGpp (**Figure**
93 **2a**). The binding is highly specific, as non-radiolabeled ppGpp effectively competes with
94 radiolabeled (p)ppGpp binding, whereas non-radiolabeled GTP failed to compete. EDTA
95 eradicated (p)ppGpp binding to His-MBP-YvcI cell lysate, which implies that the divalent
96 cations present in the reaction is essential for (p)ppGpp binding to YvcI (**Figure 2a**).

97 Even though YvcI overexpression cell lysate showed strong and specific binding
98 to (p)ppGpp, the purified protein does not appear to bind (p)ppGpp in DRaCALA **(Figure**
99 **S2)**. This can be due to two possibilities. Either YvcI requires a co-factor present in the
100 lysate to bind to (p)ppGpp; alternatively, YvcI may rapidly hydrolyse the (p)ppGpp and
101 release the product. Therefore, we incubated purified YvcI with [5'-α-$^{32}$P]-(p)ppGpp and
102 ran the reaction product using TLC (**Figure S3**). We found that YvcI can hydrolyze both
103 ppGpp and pppGpp, but not GTP. The inability of YvcI to hydrolyze GTP and the strong
104 structural similarity between GTP and (p)ppGpp suggest that SatA is a specific (p)ppGpp
105 hydrolase which requires its substrate to have pyrophosphate group on the 3′ end.
106 However, unlike *B. subtilis* RelA, which hydrolyzes the 3'-pyrophosphate group from
107 ppGpp and pppGpp to produce GDP and GTP, SatA hydrolyzed ppGpp and pppGpp to
108 yield a single nucleotide species that migrated differently than GTP (**Figure S3a**) or GDP
109 (**Figure S3b**). To determine the identity of YvcI's (p)ppGpp hydrolysis product, we
110 analyzed a sample by liquid chromatography coupled with mass spectrometry (LC-MS),
111 revealing a peak of the same mass over charge ratio (m/z) as GTP but with a longer
112 retention time (11.75 min versus 11.15 min for GTP). When we ran a pGpp sample
113 produced by *E. faecalis* SAS [20], we found that it ran with the same retention time and
114 molecular weight (**Figure 2b**), suggesting that the hydrolysis product of YvcI is pGpp.

115 The production of pGpp from pppGpp and ppGpp agrees with the NuDiX
116 hydrolase function, inferring that pppGpp and ppGpp are hydrolyzed between the 5'-α
117 and 5'-β phosphate groups to produce guanosine-5'-monophosphate-3'-diphosphate
118 (pGpp). Therefore, we renamed the enzyme SatA (Small alarmone
119 (guanosine)triphosphate synthase A).

120 It is possible, although unlikely, that SatA hydrolyzes the 3′-phosphate to produce
121 ppGp, which would run at the same retention time as pGpp in LC-MS. To distinguish
122 these two possibilities, we analyzed the SatA cleavage products of [3′-β-$^{32}$P]-pppGpp. If
123 SatA cleaves the 5'-γ and β phosphates, the reaction would yield [3′-β-$^{32}$P]-pGpp. (In
124 contrast, if Sat A cleaves the 3'-β-phosphate and the 5'-γ-phosphate, the reaction would
125 yield free $^{32}$P-phosphate). TLC analysis revealed that the radioactive $^{32}$P after SatA
126 hydrolysis of [3′-β-$^{32}$P]-pppGpp co-migrates with the pGpp nucleotide rather than free
127 phosphate that migrates to the very end of TLC plate (**Figure 2c**). This result showed
128 that the product has an intact 3'-pyrophosphate group, confirming the product to be
129 pGpp rather than ppGp. Moreover, quantification of [3′-β-$^{32}$P]-pppGpp hydrolysis by SatA
130 showed that the decrease of substrate radioactivity mirrored the increase of the single
131 product radioactivity (**Figure 2d**), demonstrating the product is exclusively pGpp.

132 As a NuDiX hydrolase, SatA has been reported to have a modest activity in
133 removing the 5'-phosphate of mRNA [24]. We found that SatA is far more efficient at
134 hydrolyzing (p)ppGpp than at decapping mRNA. Enzymatic assays revealed that SatA
135 hydrolyzes ppGpp following Michaelis-Menten kinetics, with a $k_{cat}$ of 1.22 ± 0.17 $s^{-1}$ and a
136 $K_m$ of 7.5 ± 2.3 μM (**Figure 2e, Table 1**). SatA also effectively and cooperatively
137 hydrolyzes pppGpp, with a Hill coefficient of 2.78 ± 0.47, $k_{cat}$ of 10.0 ± 0.5 $s^{-1}$ and $K_m$ of
138 177.4 ± 0.4 μM (**Figure 2e, Table 1**). In contrast, its $k_{cat}$ to decap RNA is around 0.0003

139 $s^{-1}$ (estimation based on published figure) [24]. The difference in $k_{cat}$ *in vitro* suggest that
140 SatA's major function is to regulate (p)ppGpp rather than to decap the 5' cap of mRNA.

141

142 **SatA hydrolyzes (p)ppGpp to produce pGpp *in vivo***

143 SatA was previously identified as a constitutively expressed protein with ~600
144 copies per cell [25]. To examine its impact on (p)ppGpp *in vivo*, we engineered a *satA*
145 deletion strain, and developed an LC-MS metabolome quantification for pppGpp, ppGpp
146 and pGpp in *B. subtilis* cells (see Material & Methods). LC-MS measurement of cell
147 extracts showed that Δ*satA* mutants accumulates more pppGpp and ppGpp than wild
148 type cells during both log phase and stationary phase, in agreement with SatA's ability to
149 hydrolyze (p)ppGpp (**Figure 3a**). In contrast, Δ*satA* mutant accumulates less pGpp than
150 wild type cells. In fact, during log phase, pGpp levels are consistently detectable in wild
151 type cells but fall below the detection limit in Δ*satA* (**Figure 3a**). When we complement
152 Δ*satA* with an overexpressed copy of *satA*, the pGpp levels were restored to wild type
153 levels (**Figure S5**). These results support the function of SatA in producing pGpp.

154 We also used the drug arginine hydroxamate (RHX) to induce accumulation of
155 (p)ppGpp[10]. Using both LC-MS and TLC, we observed rapid accumulation of (p)ppGpp
156 after RHX treatment, with Δ*satA* cells showing stronger (p)ppGpp accumulation than wild
157 type cells (**Figure S4a-d)**. We still observe the accumulation of pGpp in Δ*satA* cells,
158 although to a much less extent than wild type cells **(Figure S4e)**, this remaining pGpp in
159 Δ*satA* cells is likely due to the function of the enzyme SAS1, which can synthesize pGpp
160 from GMP and ATP[26].

161

162 **pGpp can be hydrolyzed by RelA *in vitro***

163 We have detected basal levels of pGpp in log phase and elevated levels of pGpp
164 in starved cells, suggesting that it is an alarmone in *B. subtilis*. Alarmones must be
165 eventually degraded for restoring bacterial growth. In *B. subtilis*, pppGpp and ppGpp are
166 both hydrolyzed by RelA, which has a functional (p)ppGpp hydrolase domain in
167 Firmicutes/Gram-positive bacteria. Therefore, we performed hydrolysis assays using
168 purified *B. subtilis* RelA and pGpp, ppGpp or pppGpp as substrates *in vitro* **(Figure 3b)**.
169 We found that all three nucleotides can be hydrolyzed efficiently by RelA, furthermore,
170 pGpp was hydrolyzed more rapidly than (p)ppGpp (**Figure 3b**).

171

172 **Protein binding spectrum of pGpp is distinct from (p)ppGpp**

173 To understand whether pGpp is just an intermediate of (p)ppGpp hydrolysis or is
174 a bona fide alarmone with its own regulatory targets, we used DRaCALA to
175 systematically screen the *B. anthracis* library for pGpp-binding targets (**Figure 1a-b**,
176 **Table S1**). Our screen showed that pGpp binds strongly to multiple purine nucleotide
177 synthesis enzymes which are also targets of (p)ppGpp (**Figure 1c**), but binds to none of
178 the (p)ppGpp-binding ribosome and translation regulation GTPases (**Figure 1d**). We
179 purified selected pGpp and (p)ppGpp binding targets and tested with [5′-α-$^{32}$P]-labeled
180 pGpp, ppGpp and pppGpp in DRaCALA (**Figure 3c-d**). This confirmed that the strongest
181 pGpp-binding targets are guanosine nucleotide synthesis proteins (Hpt1, Gmk, Xpt).
182 This also confirmed that GTPases involved in ribosome biogenesis bound by (p)ppGpp
183 (HflX, Obg, Der) were not bound by pGpp (**Figure 3c-e**). The $K_d$ of (p)ppGpp binding to
184 these GTPases (**Table S2**) showed their strong affinity to ppGpp, mediocre affinity to
185 pppGpp and lack of affinity to pGpp. Since these GTPases play important roles in
186 translational regulation, these results imply that pGpp does not directly regulate
187 translation unlike pppGpp and ppGpp.

188

189 **Loss of *satA* in *Bacillus* leads to stronger inhibition of translation upon amino**
190 **acid starvation, delayed outgrowth and loss of competitive fitness**

191 Δ*satA* showed increased accumulation of (p)ppGpp and reduced levels of pGpp
192 **(Figure 3a)**. The fact that pGpp strongly regulates purine synthesis but does not directly
193 regulate ribosome biogenesis and translation implicates an *in vivo* function of SatA:
194 reducing (p)ppGpp levels to alleviate translation inhibition upon stress, while still keeping
195 purine biosynthesis in check. To test this hypothesis, we measured total protein
196 translation rate of wild type and Δ*satA B. subtilis* by incorporation of $^{35}$S-methionine. We
197 found that after RHX treatment, the rate of $^{35}$S-methionine incorporation is significantly
198 more strongly reduced in Δ*satA* than in wild type ($P<0.05$), indicating a stronger
199 inhibition of translation (**Figure 4a**).

200 Next, we examined the impact of *satA* on fitness of *B. subtilis*. In a growth
201 competition assay, the CFU ratio between Δ*satA* and wild type cells steadily decreased
202 over time (**Figure 4b**). The calculated relative fitness of Δ*satA* is 0.875 ± 0.008 (mean ±
203 S.D.), indicating significant loss of fitness due to *satA* deletion. We found that Δ*satA* has
204 a similar doubling time as wild type cells, but has a longer lag phase during outgrowth
205 upon amino acid downshift (**Figure 4c-d**). Together, these results suggest that SatA
206 tunes alarmone composition and alarmone levels to promote *B. subtilis* adjustment to
207 nutrient fluctuation and optimizes growth and fitness.

208

209 **Discussion**

210 Alarmones are universal stress signaling nucleotides in bacteria, however, the
211 repertoire of alarmones and the target spectrums for each alarmone are incompletely

212 understood. In this work, we have comprehensively characterized the interactomes of
213 the related alarmones pppGpp and ppGpp and established the *in vivo* presence of pGpp
214 as a closely related alarmone in Gram-positive *Bacillus* species. We characterized the
215 direct targets of (p)ppGpp by screening an open reading frame expression library from
216 *B. anthracis*. From this screen, we identified an enzyme SatA that converts (p)ppGpp to
217 pGpp as efficient means to produce pGpp and to reduce (p)ppGpp concentrations, thus
218 regulating the composition of the alarmones. We demonstrated that pGpp binds a
219 distinct subset of protein receptors of (p)ppGpp in *Bacillus* species. The key role of SatA
220 in nutrient adaptation suggests that regulating alarmone composition may serve as a
221 separation-of-function strategy for optimal adaptation.

222

223 **Conservation of (p)ppGpp regulation of purine biosynthesis and ribosome**
224 **biogenesis pathways across different species of bacteria**

225 (p)ppGpp regulates diverse cellular targets that differ between different bacteria.
226 For example, (p)ppGpp directly binds to RNA polymerase in *E. coli* to control the
227 transcription of ribosomal and tRNA operons yet the (p)ppGpp binding sites on RNA
228 polymerase are not conserved beyond proteobacteria[4,5]. Instead, (p)ppGpp
229 accumulation in firmicutes strongly down-regulates synthesis of GTP, the exclusive
230 transcription initiating nucleotides of rRNA and tRNA operons in firmicutes, to achieve a
231 similar transcription control with different direct targets[10,27,28]. Therefore, identifying
232 whether certain aspects of (p)ppGpp regulation are conserved among bacterial species
233 is important for understanding bacterial survival and adaptation.

234 Our DRaCALA screen with a *B. anthracis* library revealed many ppGpp and
235 pppGpp binding targets in this pathogenic Gram-positive bacterium. Comparison to

236 ppGpp-binding targets in *B. anthracis* to *S. aureus*[16] and *E. coli*[13,18] identified novel
237 targets but more importantly, revealed a clear theme of conservation. Most notably,
238 (p)ppGpp in all three species binds to multiple proteins in two key pathways: 1) purine
239 nucleotide synthesis, 2) translation-related GTPases including ribosome biogenesis
240 factors.

241 The regulation of purine nucleotide synthesis in firmicutes includes well
242 characterized targets Gmk and HprT whose regulation by (p)ppGpp protects *Bacillus*
243 *subtilis* against nutrient changes like amino acid starvation and purine fluctuation,
244 preventing cells from accumulating toxic high levels of intracellular GTP[10,12,29]. These
245 also include new-found likely targets such as enzymes GuaC and PurA and the *de novo*
246 pathway transcription factor PurR. Intriguingly, in the evolutionarily distant *E. coli*, the
247 ppGpp targets in the purine biosynthesis pathway are different. For example, Gmk is not
248 regulated by (p)ppGpp in *E. coli*. On the other hand, (p)ppGpp directly targets the *de*
249 *novo* enzyme PurF[13], a target that is not conserved in firmicutes. Therefore, despite
250 differences in precise targets, (p)ppGpp extensively regulates the purine biosynthesis
251 pathway in evolutionarily diverse bacteria **(Figure 1c),** highlighting this critical
252 physiological role of (p)ppGpp.

253 (p)ppGpp also interacts with essential GTPases that are implicated in ribosome
254 biogenesis **(Figure 1d)**[16]. In contrast to the diversification of direct targets in purine
255 biogenesis, (p)ppGp's targets in GTPases from *E. coli* to firmicutes are conserved. This
256 can be due to the structural similarity between GTP/GDP and pppGpp/ppGpp, which
257 allows (p)ppGpp to bind to the GTP/GDP binding sites, respectively. The conservation of
258 ribosome biogenesis targets implicates the importance of translational control in stress
259 responses across bacteria.

260

261 **The third major alarmone pGpp in Gram positive species and its specific**
262 **regulatory effect**

263 In addition to pppGpp and ppGpp, it was long suspected that in *B. subtilis*, there are
264 additional alarmones such as pppApp, pGpp, and ppGp accumulating during the
265 stringent response [30,31]. However, their sources, mechanisms and targets are poorly
266 characterized. Here we detected pGpp in *B. subtilis* cells, characterized an enzyme for
267 its production *in vivo* and *in vitro*, and identified its targets. In contrast to our DRaCALA
268 screens for pppGpp and ppGpp which identify similar targets and functionalities between
269 these two alarmones, DRaCALA screen for pGpp displays a strong difference from
270 (p)ppGpp with regarding to two conserved pathways. The affinity of pGpp for purine
271 nucleotide synthesis proteins is equivalent or higher than that of (p)ppGpp. In contrast,
272 pGpp's affinity to GTPases involved in translational regulation is much lower, or
273 insignificant, compared to (p)ppGpp. The distinct profile of target receptors distinguish
274 pGpp as a different alarmone from (p)ppGpp, potentially allowing fine tuning of bacterial
275 stress response. We propose a model for the function of SatA in growth recovery and
276 competitive fitness by its role in transforming the alarmones. In wild type cells, (p)ppGpp
277 produced in response to amino acid starvation will be hydrolyzed in part by SatA to
278 pGpp. (p)ppGpp concentration in wild type cells during amino acid starvation can reach
279 ~1 mM, which is well above the $K_M$ of (p)ppGpp for SatA and suggests SatA should be at
280 its maximum velocity. Given the copy number of SatA as ~600 copies per cell and its
281 maximum velocities for (p)ppGpp hydrolysis, intracellular SatA can hydrolyze ~6000
282 molecules of pppGpp and ~600 molecules of ppGpp per second. This corresponds to a
283 pppGpp hydrolysis rate of 6 μM/s and ppGpp hydrolysis rate of 0.6 μM/s (assuming 1
284 $\mu m^3$ intracellular volume). In 30 minutes, SatA can hydrolyze 10.8 mM pppGpp and 1.08
285 mM ppGpp. Clearly, SatA does not hydrolyze all pppGpp and ppGpp likely because

286 RelA replenishes the alarmones. We propose that (p)ppGpp concentrations observed in
287 wild type cells is a balance of RelA synthesis and SatA hydrolysis. Thus, in Δ*satA* cells,
288 (p)ppGpp accumulates higher than in wild type cells during amino acid starvation.
289 Stronger inhibition of translation due to overly high level of (p)ppGpp in Δ*satA* leads to
290 slower growth recovery after culture enduring nutrient downshift and thus may lead to
291 fitness loss when co-cultured with wild type strain. In addition, because pGpp is
292 hydrolyzed much more efficiently by RelA (**Figure 3b**), another benefit of SatA is
293 perhaps to speed up (p)ppGpp removal to promote recovery.

294 In *E. coli*, (p)ppGpp binding proteins also include NuDiX hydrolases NudG and
295 MutT[18]. Like SatA, NudG and MutT also hydrolize (p)ppGpp. Unlike SatA, NudG and
296 MutT produce guanosine 5'-monophosphate 3'-monophosphate (pGp) rather than pGpp.
297 Sequence alignment shows that *E. coli* NudG and MutT shares only marginal homology
298 with SatA proteins: the homology is almost restricted in the NuDiX box that is shared by
299 NuDiX hydrolase family (**Figure S1**). Therefore, NudG and MutT are considered
300 alternative (p)ppGpp hydrolysis pathways in addition to the SpoT hydrolase, rather than
301 an alarmone-producer.

302 In *E. coli*, the enzyme GppA converts pppGpp to ppGpp, which may also regulate
303 the composition of its alarmones[19]. In the absence of GppA, the alarmone pppGpp
304 accumulates to a higher level than ppGpp[32]. It is possible that a similar separation-of-
305 function regulation exists in *E. coli* by tuning pppGpp vs ppGpp levels. This can be
306 addressed by examining pppGpp interactome in *E. coli*, which may reveal a differential
307 theme than ppGpp. Ultimately, discovery of more enzymes that interconvert signaling
308 molecules may reveal a universal theme of optimization through fine-tuning in signal
309 transduction.

310

311 **Acknowledgement**

312 We thank Mona Orr and David Stevenson for technical help. This work is supported, in
313 part, by an R35 GM127088 from NIGMS (to JDW), a GRFP DGE-1256259 from NSF (to
314 BWA) and R01AI110740 from NIAID and NIDDK (to VTL).

315

316 **Materials and Methods**

317 ***Bacillus anthracis* ORFeome Library Construction**

318 *Bacillus anthracis* Gateway® Clone Set containing plasmids bearing *B. anthracis* open
319 reading frames was acquired from BEI Resources and used for Gateway cloning
320 (Invitrogen protocol) into overexpression vectors pVL791 (10xHis tag ampicillin-resistant)
321 and pVL847 (10xHis-MBP tag, gentamycin-resistant) and transformed into *Escherichia*
322 *coli* BL21 $lacI^q$ to produce two open reading frame proteome over-expression libraries
323 (ORFeome library). The resulting ORFeome library contains 5139 ORFs from the
324 genome of *B. anthracis str. Ames* (91.2% of 5632 ORFs in the genome). The
325 corresponding proteins were expressed in *E. coli* and the cells were lysed to prepare the
326 overexpression lysates for the downstream analysis.

327 **Plasmid and Strain Construction and Growth Conditions**

328 Plasmid for SatA purification was constructed as follows: *satA* encoding sequence was
329 PCR amplified and incorporated into pE-SUMO vector by Golden Gate assembly
330 method (New England BioLabs), and into pVL847 (His-MBP-tag overexpression vector)
331 by Gateway cloning method (Invitrogen). Δ*satA* mutant of *Bacillus subtilis* was
332 constructed by CRISPR/Cas9 editing method (Ref). Primers for plasmid construction

333 and mutation verification are listed in (**Table S3**). *satA* deletion was confirmed by DNA
334 sequencing.

335 If not specifically mentioned, *B. subtilis* strains were grown in S7 defined media [33] with
336 modifications (50 mM MOPS instead of 100 mM, 0.1% potassium glutamate, 1%
337 glucose, no additional tryptophan or methionine) , with shaking at 250 rpm 37˚C. The
338 modified S7 defined media with 20 amino acids contains 50 µg/mL alanine, 50 µg/mL
339 arginine, 50 µg/mL asparagine, 50 µg/mL glutamine, 50 µg/mL histidine, 50 µg/mL
340 lysine, 50 µg/mL proline, 50 µg/mL serine, 50 µg/mL threonine, 50 µg/mL glycine, 50
341 µg/mL isoleucine, 50 µg/mL leucine, 50 µg/mL methionine, 50 µg/mL valine, 50 µg/mL
342 phenylalanine, 500 µg/mL aspartic acid, 500 µg/mL glutamic acid, 20 µg/mL tryptophan,
343 20 µg/mL tyrosine, and 40 µg/mL cysteine.

344 **Nucleotide Preparation**

345 (p)ppGpp was synthesized *in vitro* using Rel*Seq*$_{1-385}$ and GppA, purified and quantified
346 as demonstrated[19]. pGpp was a gift from José A. Lemos Lab in University of Rochester
347 Medical Center.

348 Radiolabeled (p)ppGpp was synthesized *in vitro* using Rel*Seq*$_{1-385}$ and GppA as
349 demonstrated[19] with modifications. We replaced non-radiolabeled GTP with 750 µCi/mL
350 $^{32}$P-α-GTP (3000 mCi / mmol; PerkinElmer) for production of [5′-α-$^{32}$P]-(p)ppGpp. We
351 replaced non-radiolabeled ATP with 750 µCi/mL $^{32}$P-γ-ATP (3000 mCi/mmol;
352 PerkinElmer) for production of [3′-β-$^{32}$P]-ppGpp. After the reaction was done, we 1:10
353 diluted the reaction mix in Buffer A (0.1 mM LiCl, 0.5 mM EDTA, 25 mM Tris pH 7.5).
354 The mixture was loaded onto a Buffer-A-equilibrated 1 mL HiTrap QFF column (GE
355 Healthcare). Then the column was washed sequentially by 10 column volumes of Buffer
356 A, and 10 column volumes of Buffer A with 170 mM LiCl (for ppGpp purification, the LiCl

357 concentration was 160 mM) with 1 mL fractions. Radiolabeled (p)ppGpp was eluted by 5
358 column volumes of Buffer A with 500 mM LiCl with 1 mL fractions. The radioactivity and
359 purity of radiolabeled (p)ppGpp were analyzed by thin-layer chromatography and
360 phosphorimaging.

361 **Overexpression and Purification of SatA**

362 pE-SUMO-SatA was transformed into E. coli BL21(DE3) $lacI^q$ by chemical
363 transformation. A single colony of the corresponding strain was grown in LB with 30
364 µg/mL kanamycin overnight. Overnight culture was 1:100 diluted in LB-M9 media (7 g/L
365 $Na_2HPO_4$, 2 g/L $KH_2PO_4$, 0.5 g/L NaCl, 1 g/L $NH_4Cl$, 2 g/L glucose, 1 g/L sodium
366 succinate dibasic hexahydrate; 10 g/L tryptone, 5 g/L yeast extract and 3 mM $MgSO_4$)
367 with 30 µg/mL kanamycin and grown at 30˚C with shaking for 4 hr. After adding 1 mM
368 IPTG for induction, the culture was further grown at 30˚C for 4 hr. Then the culture was
369 centrifuged at 4000 g for 30 min at 4˚C and the supernatant was discarded. The pellet
370 was stored at -80˚C before cell lysis. All the following steps were performed at 4˚C. Pellet
371 was re-suspended in Lysis Buffer (50mM Tris-HCl pH 8, 10% sucrose w/v, 300mM
372 NaCl) and lysed by French press. Cell lysate was centrifuged at 15000 rpm for 30 min,
373 and the supernatant was collected, filtered through 0.45 µm pore-size cellulose syringe
374 filter. His-SUMO-SatA filtered supernatant was purified using a 5 mL HisTrap FF column
375 (GE Healthcare) equipped on an ÄKTA FPLC apparatus (GE Healthcare). SUMO Buffer
376 A (50 mM Tris-HCl, 25 mM imidazole, 500 mM NaCl, 5% glycerol v/v) was used as
377 washing buffer, and SUMO Buffer C (50 mM Tris-HCl, 500 mM imidazole, 500 mM NaCl,
378 5% glycerol v/v) was used as the elution buffer. Fractions containing most abundant His-
379 SUMO-SatA were combined with 100 µg SUMO Protease and dialyzed twice against
380 SUMO Protease Buffer (50 mM Tris-HCl, 500 mM NaCl, 5% glycerol v/v, 1 mM β-

381 mercaptoethanol) overnight. His-SUMO tag was removed by flowing through HisTrap FF
382 column and collecting the flow-through. Purified SatA was analyzed by SDS-PAGE and
383 the concentration was measured by the Bradford assay (Bio-rad).

384 **Differential Radial Capillary Action Ligand Assay (DRaCALA)**

385 Cell lysate with overexpressed protein and purified protein were used for DRaCALA as
386 described[22]. 10 µL cell lysate or diluted, purified protein was mixed with 10 µL diluted [5′-
387 α-$^{32}$P]-(p)ppGpp (~0.2 nM) in a buffer containing 10 mM Tris pH 7.5, 100 mM NaCl and 5
388 mM $MgCl_2$, incubated at room temperature for 10 min. ~2 µL mixture was blotted onto
389 nitrocellulose membrane (Amersham; GE Healthcare) and allowed for diffusion and
390 drying. The nitrocellulose membrane loaded with mixture was exposed on phosphor
391 screen, which was scanned by a Typhoon FLA9000 scanner (GE Healthcare). Fraction
392 of (p)ppGpp binding was analyzed as described[22].

393 **Quantification of Intracellular Nucleotides by Thin-Layer Chromatography**

394 Quantification of ATP, GTP, and (p)ppGpp levels by thin-layer chromatography was
395 performed as described before [34,35] with modifications. Cells were grown in low
396 phosphate S7 defined media (0.5 mM phosphate instead of 5 mM), labeled with 50
397 µCi/mL culture decontaminated $^{32}$P-orthophosphate (9000 mCi/mmol; Perkin-Elmer)
398 (decontamination was performed as demonstrated previously[36]) at an optical density at
399 600 nm ($OD_{600nm}$) of ~0.01 and grown for two to three additional generations before
400 sampling. Nucleotides were extracted by adding 100 µL of sample into 20 µL 2 N formic
401 acid on ice for at least 20 min. Extracted samples were centrifuged at 15,000 g for 30
402 min to remove cell debris. Supernatant samples were spotted on PEI cellulose plates
403 (EMD-Millipore) and developed in 1.5 M or 0.85 M potassium phosphate monobasic
404 ($KH_2PO_4$) (pH 3.4). TLC plates were exposed on phosphor screens, which were scanned

405 by a Typhoon FLA9000 scanner (GE Healthcare). Nucleotide levels were quantified by
406 ImageJ (NIH). Nucleotide levels are normalized to ATP level at time zero.

407 **Kinetic Assay of (p)ppGpp Hydrolysis by SatA**

408 100 μL reaction mix was prepared with 40 mM Tris HCl pH 7.5, 100 mM NaCl, 10 mM
409 $MgCl_2$, non-radioactive and $^{32}P$-radiolabeled (p)ppGpp (concentration as required by
410 specific experiments), 100 nM purified SatA (add enzyme last). Before adding enzyme,
411 reaction mix was prewarmed at 37℃ for at least 10 min. After adding enzyme, 10 μL
412 reaction mix was aliquoted into 10 μL ice-chilled 0.8 M formic acid to stop the reaction
413 and preserve nucleotides at every time point. Samples at each time point were resolved
414 by thin-layer chromatography on PEI-cellulose plates with 1.5 M $KH_2PO_4$ (pH 3.4).
415 Nucleotide levels were quantified as mentioned above and the phosphorimager counts
416 of substrate and product were used to calculate the concentration of product by a
417 formula:

418 $$c_P = c_{S0} \cdot \frac{V_P}{V_P + V_S}$$

419 Here $c_P$ was the concentration of product, $c_{S0}$ was the concentration of substrate before
420 the reaction starts, $V_P$ was the phosphorimager count of product, and $V_S$ was the
421 phosphorimager count of substrate. Initial rates of hydrolysis ($v_0$) were calculated using
422 the slope of the initial linear part of $c_P$ over time curve at different initial substrate
423 concentrations. Michaelis-Menten constant ($K_m$) and catalytic rate constant ($k_{cat}$) were
424 obtained by fitting the data of $v_0$-$c_{S0}$ to the model

425 $$v_0 = \frac{c_E \cdot k_{cat} \cdot c_{S0}^n}{K_m^n + c_{S0}^n}$$

426 by MATLAB, where $c_E$ was the concentration of SatA, $c_{S0}$ was the initial concentration of
427 substrate, and $n$ was the Hill's coefficient (for ppGpp hydrolysis, fix $n$ to 1).

428 **LC-MS Quantification of Nucleotides**

429 LC-MS quantification of nucleotides was performed as described[29] with modifications.
430 Cells were grown to designated $OD_{600nm}$. 5 mL of cultures were sampled and filtered
431 through PTFE membrane (Sartorius) at time points before and after 0.5 mg/mL arginine
432 hydroxamate treatment. Membranes with cell pellet were submerged in 3 mL extraction
433 solvent mix (on ice 50:50 (v/v) chloroform/water) to quench metabolism, lyse the cells
434 and extract metabolites. Mixture of cell extracts were centrifuged at 5000 g for 10 min to
435 remove organic phase, then centrifuged at 20000 g for 10 min to remove cell debris.
436 Samples were frozen at -80℃ if not analyzed immediately. Samples were analyzed
437 using HPLC-MS system consisting of a Vanquish UHPLC system linked to electrospray
438 ionization (ESI, negative mode) to a Q Exactive Orbitrap mass spectrometer (Thermo
439 Scientific) operated in full-scan mode to detect targeted metabolites based on their
440 accurate masses. LC was performed on an Aquity UPLC BEH C18 column (1.7 μm, 2.1
441 X 100 mm; Waters). Total run time was 30 min with a flow rate of 0.2 mL/min, using
442 Solvent A (97:3 (v/v) water/methanol, 10 mM tributylamine and 10 mM acetic acid) and
443 acetonitrile as Solvent B. The gradient was as follows: 0 min, 5% B; 2.5 min, 5% B; 19
444 min, 100% B; 23.5 min 100% B; 24 min, 5% B; 30 min, 5% B. Quantification of
445 metabolites were performed by using MAVEN software.

446 **Competition Assay**

447 LB broth cultures of erythromycin-sensitive and erythromycin-resistant strains were
448 diluted and mixed in fresh LB broth to an $OD_{600nm}$ of 0.03; the mixture was incubated at

449 37˚C at 250 rpm; after every 24 hrs the culture was diluted in fresh LB broth to an
450 $OD_{600nm}$ of 0.02 to initiate the recovery from late stationary phase; the culture was
451 sampled, serially diluted and spread over LB agar and LB agar containing 0.5 μg/mL
452 erythromycin and 12.5 μg/mL lincomycin (LB-mls agar). CFU calculated from LB agar
453 and LB-mls agar represented the CFU of total bacteria and erythromycin-resistant strain,
454 respectively. Relative fitness was calculated by the formula: $w = \frac{log_2(CFU_{erm^R{}_t}/CFU_{erm^R{}_0})}{log_2(CFU_{erm^S{}_t}/CFU_{erm^S{}_0})}$,
455 where w means relative fitness of the erythromycin-resistant strain to the erythromycin-
456 sensitive strain; $CFU_{erm^R{}_0}$ and $CFU_{erm^R{}_t}$ means the total CFU of erythromycin-resistant
457 strain before and after competition, respectively; $CFU_{erm^S{}_0}$ and $CFU_{erm^S{}_t}$ means the total
458 CFU of erythromycin-sensitive strain before and after competition, respectively.

459 **[$^{35}$S]-Methionine Incorporation Assay**

460 [$^{35}$S]-Methionine (10.2 mCi/mL, PerkinElmer) was diluted to 0.5 μCi/μL and aliquoted into
461 1.5 mL Eppendorf tubes (10 μL per tube, heated at 37℃). Cells were grown to $OD_{600nm}$
462 at around 0.2 (record the exact OD). Aliquots of 200 μL culture were taken at time points
463 before and after 0.5 mg/mL RHX treatment, added into tubes of aliquoted [$^{35}$S]-
464 Methionine, incubated at 37˚C for 5 min and fixed by adding 200 μL ice-chilled 20% (w/v)
465 trichloroacetic acid. Fixed samples were chilled before filtration. Glass fiber filters
466 (24mm, GF6, Whatman) were prewetted with 3 mL ice-chilled 5%(w/v) trichloroacetic
467 acid and applied with fixed samples. Filters were then washed three times by 3 x 10 mL
468 ice-chilled 5%(w/v) trichloroacetic acid and dried by ethanol. Dried filters were put in
469 scintillation vials, mixed with 5 mL scintillation fluid and then sent for scintillation count in
470 the range of 2.0-18.6 eV. Counts per minutes (CPM) measured by scintillation counter
471 were used as the representative of translation rate. The ratio of the CPM of one sample
472 relative to the CPM at time zero was calculated as the relative translation rate.

473 **Out growth from nutrient downshift**

474 Cells were grown in rich medium (S7 + 20 amino acids) to mid log phase, and then
475 washed in poor medium (S7 without amino acid). Washed cultures were diluted into
476 fresh rich medium and the growth was monitored by a plate reader (Synergy 2, Biotek)
477 at 37˚C under shaking.

478 **Figure 1. Proteome-wide DRaCALA screen identifies both conserved categories of**
479 **binding targets and novel targets.**

480 **a)** The *Bacillus anthracis* ORF donor vector library was recombined by Gateway cloning
481 into overexpression vectors to generate ORFs with an N-terminal His-tag or His-MBP
482 tag. The plasmids were transformed into *E. coli* for overexpression of recombinant
483 proteins. Lysates of each ORF overexpressed in *E. coli* were assayed for binding to
484 pppGpp, ppGpp and pGpp using DRaCALA. **b)** List of identified (p)ppGpp binding
485 targets in *E. coli*, *S. aureus,* and *B. anthracis* and pGpp binding targets in *B. anthracis*.
486 **c-d)** Schematics of pathways differentially regulated by pGpp and (p)ppGpp: **c)**
487 Enzymes in purine nucleotide synthesis, including HprT, Xpt, Gmk and GuaC, bound
488 both pGpp and (p)ppGpp; **d)** GTPases, involved in ribosome biogenesis and
489 translational control (Obg, HflX, Der, RbgA and Era), bound (p)ppGpp, but not pGpp.

490 **Figure 2. SatA (YvcI) produces pGpp via (p)ppGpp hydrolysis.**

491 **a)** DRaCALA of [5'-α-$^{32}$P]-ppGpp binding to *B. subtilis* HisMBP labeled -YvcI (SatA)
492 overexpressed in *E. coli* cell lysate. Unlablled GTP (100 uM), unlabeled ppGpp (100 μM)
493 and EDTA (10 mM) were added as indicated. **b)** Ion count vs. retention time curves from
494 LC-MS of GTP and pGpp standards and SatA-catalyzed hydrolysis products from ppGpp
495 and pppGpp. **c)** TLC analysis of SatA activity over time with [3′-β-$^{32}$P]-pppGpp.
496 Expected SatA-catalyzed conversion of [3′-β-$^{32}$P]-pppGpp to [3′-β-$^{32}$P]-pGpp is shown on
497 the right. Radiolabeled [3′-β-$^{32}$P]-phosphorus atom is highlighted in red. **d)** Quantitation
498 of pppGpp and pGpp in the hydrolysis of pppGpp in (c). **e)** Initial velocity vs. pppGpp or
499 ppGpp concentration curves for SatA synthesis of pGpp. Data were obtained by kinetic
500 assay using radiolabels (see Methods). Curves represent the best fit of the data from
501 three independent experiments. Error bars represent standard error of the mean.

502

503

504 **Figure 3. pGpp is produced by SatA *in vivo* and has a distinct binding spectrum**
505 **compared to (p)ppGpp.**

506 **a)** LC-MS analyses of metabolomes of wild type and Δ*satA* in log phase and stationary
507 phase. Normalized ion count is ion count per $OD_{600}$ per unit volume of the culture. Error
508 bars represent standard error of the mean of three biological replicates. A two-tailed two-
509 sample equal-variance Student's *t* test was performed between samples indicated by
510 asterisks. Asterisks indicate statistical significance of differences (* $P \leqslant 0.05$, ** $P \leqslant 0.01$,
511 *** $P \leqslant 0.001$). **b)** RelA hydrolysis of pGpp, ppGpp and pppGpp over time. For each
512 nucleotide, 200 nM RelA was incubated with a mix of 100 μM unlabeled alarmone and a
513 small amount of 5'-α-$^{32}$P-labeled version. The degradation of the alarmone was analyzed
514 by TLC to measure the decreased radioactivity. Error bars represent standard error of
515 the mean of three technical replicates. **c)** DRaCALA of purified His-MBP-tagged *B.*
516 *anthracis* proteins (1 μM) with 5'-α-$^{32}$P-labeled pGpp, ppGpp, and pppGpp. **d)** (Upper left
517 panel) Quantification of 3 technical replicates of DRaCALA as shown in (c).
518 Quantification of 2 technical replicates of DRaCALA of purified His-MBP-tagged *B.*
519 *anthracis* GTPases HflX (upper right panel), Obg (lower left panel) and translation
520 elongation factor G (EF-G) (lower right panel). Error bars represent standard errors of
521 the mean. **e)** Schematic showing the relationship between pGpp binding targets and
522 (p)ppGpp binding targets.

523

524 **Figure 4. The effect of SatA on translation, growth recovery and fitness of *B.***
525 ***subtilis*. a)** [$^{35}$S]-methionine incorporation assay of wild type and Δ*satA* strains after
526 arginine hydroxamate (RHX) treatment at t=0. Error bars represent standard errors of
527 the mean from three replicates. A two-tailed two-sample equal-variance Student's *t* test
528 was performed between samples indicated by asterisks. Asterisk indicates statistical
529 significance of difference (* $P \leqslant 0.05$). **b)** Change of percentage of Δ*satA::erm* and wild
530 type strains in total colony forming units (CFU) during a competition assay in LB broth
531 over time. Error bars represent standard errors of the mean from 3 repeats. **c)** Out
532 growth from nutrient downshift. Log phase cultures of wild type, Δ*satA* and *satA*
533 complementation strains in rich media were firstly washed in minimum media without
534 amino acids, and then diluted in rich media for outgrowth. **d)** Doubling times during log
535 phase of outgrowth shown in (c). Error bars in (c-d) represent standard errors from 6
536 replicates.

537

538 **Figure S1. Protein sequence alignment of SatA (YvcI) homologs in different**

539 **species.**

540 Multiple sequence alignment of YvcI homologs from *B. subtilis* (Bsub), *B. anthracis*

541 (Ban), *B. halodurans* (Bhalo), and *E. coli* (Ec). Alignment was obtained with MAFFT. Red

542 shading indicates identical residues in all sequences and orange shading indicates

543 identical residues only in *Bacillus* species. Red dots label the key residues for catalytic

544 activity. Numbers on the sides of the sequences indicate the residue numbers in the

545 corresponding proteins.

546 **Figure S2. Cell lysate containing YvcI, but not purified YvcI, binds (p)ppGpp.**

547 DRaCALA of cell lysate containing His-MBP-tagged *B. subtilis* YvcI(SatA) and purified

548 His-MBP-tagged *B. subtilis* YvcI(SatA) with 5'-α-$^{32}$P-labeled (p)ppGpp.

549

550 **Figure S3. SatA hydrolyzes (p)ppGpp *in vitro*.**

551 **a)** TLC analysis of pppGpp and ppGpp hydrolysis by SatA over time. The same assay
552 was also performed using GTP. **b)** TLC analysis of ppGpp hydrolysis by RelA and SatA
553 over time. Substrate and product identities are labeled on the left side of the figure.

554

555 **Figure S4. SatA hydrolyzes (p)ppGpp *in vivo* in *B. subtilis* treated by arginine**
556 **hydroxamate.**

557 **a-b)** pppGpp (a) and ppGpp (b) levels in wild type and Δ*satA B. subtilis* treated with
558 arginine hydroxamate (RHX). Nucleotide levels were assayed via TLC and are
559 normalized to the ATP level at time zero ($ATP_{t=0}$). Error bars represent standard errors of
560 mean of three independent experiments. **c-e)** LC-MS analyses of pppGpp (c), ppGpp (d)
561 and pGpp (e) of wild type and Δ*satA* before and after RHX treatment. Normalized ion
562 count is ion count per $OD_{600}$ per unit volume of the culture. Error bars represent standard
563 error of the mean of two biological replicates. Asterisks indicate statistical significance of
564 differences (* $P \leqslant 0.05$, ** $P \leqslant 0.01$).

565

566 **Figure S5. *satA* complementation rescues pGpp production *in vivo*.**

567 **a)** Intensity profile of pGpp m/z ratio from LC-MS profiling of mid log phase wild type,
568 Δ*satA* and *satA* ectopic complementation strain (Δ*satA amyE::Phy::satA*). For each
569 strain, a representative curve was shown. Dashed lines are the shoulders of the GTP
570 signal peak. **b)** Normalized ion count (ion count per $OD_{600}$ per unit volume of the culture)
571 of corresponding pGpp levels, obtained as the average of 3 biological replicates in **a)**.
572 Error bars represents standard error of the mean.

573

574 **References**


575 1. Cashel, M. The stringent response. in *Escherichia coli and Salmonella Molecular*
576 *and Cell Biology* 1485–1496 (1996).

577 2. Liu, K., Bittner, A. N. & Wang, J. D. Diversity in (p)ppGpp metabolism and
578 effectors. *Curr. Opin. Microbiol.* **24**, 72–79 (2015).

579 3. Dalebroux, Z. D., Svensson, S. L., Gaynor, E. C. & Swanson, M. S. ppGpp
580 conjures bacterial virulence. *Microbiol. Mol. Biol. Rev.* **74**, 171–199 (2010).

581 4. Ross, W., Vrentas, C. E., Sanchez-Vazquez, P., Gaal, T. & Gourse, R. L. The
582 magic spot: a ppGpp binding site on E. coli RNA polymerase responsible for
583 regulation of transcription initiation. *Mol. Cell* **50**, 420–429 (2013).

584 5. Ross, W. *et al.* ppGpp binding to a site at the RNAP-DksA interface accounts for
585 its dramatic effects on transcription initiation during the stringent response. *Mol.*
586 *Cell* **62**, 811–823 (2016).

587 6. Molodtsov, V. *et al.* Allosteric effector ppGpp potentiates the inhibition of transcript
588 initiation by DksA. *Mol. Cell* **69**, 828–839 (2018).

589 7. Wang, J. D., Sanders, G. M. & Grossman, A. D. Nutritional control of elongation of
590 DNA replication by (p)ppGpp. *Cell* **128**, 865–875 (2007).

591 8. Rymer, R. U. *et al.* Binding mechanism of metal·NTP substrates and stringent-
592 response alarmones to bacterial DnaG-type primases. *Structure* **20**, 1478–1489
593 (2012).

594 9. Maciag-Dorszyńska, M., Szalewska-Pałasz, A. & Wegrzyn, G. Different effects of
595 ppGpp on *Escherichia coli* DNA replication in vivo and in vitro. *FEBS Open Bio* **3**,
596 161–164 (2013).

597 10. Kriel, A. *et al.* Direct regulation of GTP homeostasis by (p)ppGpp: a critical
598 component of viability and stress resistance. *Mol. Cell* **48**, 231–241 (2012).

599 11. Liu, K. *et al.* Molecular mechanism and evolution of guanylate kinase regulation
600 by (p)ppGpp. *Mol. Cell* **57**, 735–749 (2015).

601 12. Anderson, B. W. *et al.* Evolution of (p)ppGpp-HPRT regulation through
602 diversification of an allosteric oligomeric interaction. *Elife* **8**, e47534 (2019).

603 13. Wang, B. *et al.* Affinity-based capture and identification of protein effectors of the
604 growth regulator ppGpp. *Nat. Chem. Biol.* **15**, 141–150 (2019).

605 14. Feng, B. *et al.* Structural and functional insights into the mode of action of a
606 universally conserved Obg GTPase. *PLoS Biol.* **12**, e1001866 (2014).

607 15. DeLivron, M. A. & Robinson, V. L. *Salmonella enterica* serovar Typhimurium BipA
608 exhibits two distinct ribosome binding modes. *J. Bacteriol.* **190**, 5944–5952
609 (2008).

610 16. Corrigan, R. M., Bellows, L. E., Wood, A. & Gründling, A. ppGpp negatively
611 impacts ribosome assembly affecting growth and antimicrobial tolerance in Gram-
612 positive bacteria. *Proc. Natl. Acad. Sci. U. S. A.* **113**, E1710–E1719 (2016).

613 17. Buglino, J., Shen, V., Hakimian, P. & Lima, C. D. Structural and biochemical
614 analysis of the Obg GTP binding protein. *Structure* **10**, 1581–1592 (2002).

615 18. Zhang, Y., Zborníková, E., Rejman, D. & Gerdes, K. Novel (p)ppGpp binding and
616 metabolizing proteins of *Escherichia coli*. *MBio* **9**, e02188-17 (2018).

617 19. Mechold, U., Potrykus, K., Murphy, H., Murakami, K. S. & Cashel, M. Differential
618 regulation by ppGpp versus pppGpp in Escherichia coli. *Nucleic Acids Res.* **41**,
619 6175–6189 (2013).

620 20. Gaca, A. O. *et al.* From (p)ppGpp to (pp)pGpp: characterization of regulatory
621 effects of pGpp synthesized by the small alarmone synthetase of Enterococcus
622 faecalis. *J. Bacteriol.* **197**, 2908–2919 (2015).

623 21. Petchiappan, A., Naik, S. Y. & Chatterji, D. RelZ-mediated stress response in
624 *Mycobacterium smegmatis*: pGpp synthesis and its regulation. *J. Bacteriol.* **202**,
625 e00444-19 (2020).

626 22. Roelofs, K. G., Wang, J., Sintim, H. O. & Lee, V. T. Differential radial capillary
627 action of ligand assay for high-throughput detection of protein-metabolite
628 interactions. *Proc. Natl. Acad. Sci. U. S. A.* **108**, 15528–15533 (2011).

629 23. Steinchen, W. *et al.* Catalytic mechanism and allosteric regulation of an oligomeric
630 (p)ppGpp synthetase by an alarmone. *Proc. Natl. Acad. Sci. U. S. A.* **112**, 13348–
631 13353 (2015).

632 24. Frindert, J. *et al.* YvcI from *Bacillus subtilis* has in vitro RNA
633 pyrophosphohydrolase activity. *J. Biol. Chem.* **294**, 19967–19977 (2019).

634 25. Maass, S. *et al.* Efficient, global-scale quantification of absolute protein amounts
635 by integration of targeted mass spectrometry and two-dimensional gel-based
636 proteomics. *Anal. Chem.* **83**, 2677–2684 (2011).

637 26. Gaca, A. O. *et al.* From (p)ppGpp to (pp)pGpp: characterization of regulatory
638 effects of pGpp synthesized by the small alarmone synthetase of *Enterococcus*
639 *faecalis*. *J. Bacteriol.* **197**, 2908–2919 (2015).

640 27. Krásný, L. & Gourse, R. L. An alternative strategy for bacterial ribosome
641 synthesis: *Bacillus subtilis* rRNA transcription regulation. *EMBO J.* **23**, 4473–4483
642 (2004).

643 28. Kriel, A. *et al.* GTP dysregulation in *Bacillus subtilis* cells lacking (p)ppGpp results
644 in phenotypic amino acid auxotrophy and failure to adapt to nutrient downshift and
645 regulate biosynthesis genes. *J. Bacteriol.* **196**, 189–201 (2014).

646 29. Liu, K. *et al.* Molecular mechanism and evolution of guanylate kinase regulation
647 by (p)ppGpp. *Mol. Cell* **57**, 735–749 (2015).

648 30. Nishino, T., Gallant, J., Shalit, P., Palmer, L. & Wehr, T. Regulatory nucleotides
649 involved in the Rel function of *Bacillus subtilis*. *J. Bacteriol.* **140**, 671–679 (1979).

650 31. Lee, P. C., Bochner, B. R. & Ames, B. N. AppppA, heat-shock stress, and cell
651 oxidation. *Proc. Natl. Acad. Sci. U. S. A.* **80**, 7496–7500 (1983).

652 32. Denapoli, J., Tehranchi, A. K. & Wang, J. D. Dose-dependent reduction of
653 replication elongation rate by (p)ppGpp in *Escherichia coli* and *Bacillus subtilis*.
654 *Mol. Microbiol.* **88**, 93–104 (2013).

655 33. Vasantha, N. & Freese, E. Enzyme changes during *Bacillus subtilis* sporulation
656 caused by deprivation of guanine nucleotides. *J. Bacteriol.* **144**, 1119–1125
657 (1980).

658 34. Bittner, A. N., Kriel, A. & Wang, J. D. Lowering GTP level increases survival of
659 amino acid starvation but slows growth rate for *Bacillus subtilis* cells lacking
660 (p)ppGpp. *J. Bacteriol.* **196**, 2067–2076 (2014).

661 35. Schneider, D. A., Murray, H. D. & Gourse, R. L. Measuring control of transcription
662 initiation by changing concentrations of nucleotides and their derivatives. in
663 *Methods in Enzymology* **370**, 606–617 (Academic Press, 2003).

664 36. Jendresen, C. B., Kilstrup, M. & Martinussen, J. A simplified method for rapid
665 quantification of intracellular nucleoside triphosphates by one-dimensional thin-

666 layer chromatography. *Anal. Biochem.* **409**, 249–259 (2011).

667

| | ppGpp | pppGpp |
|---|---|---|
| $k_{cat}$ ($s^{-1}$) | 1.22 ± 0.17 | 10.0 ± 0.5 |
| $K_M$ (μM) | 7.5 ± 2.3 | 177.4 ± 0.4 |
| Hill coefficient | 1 | 2.78 ± 0.47 |

Table 1. Kinetic parameters of (p)ppGpp hydrolysis by SatA.

Fig. 1

**a**

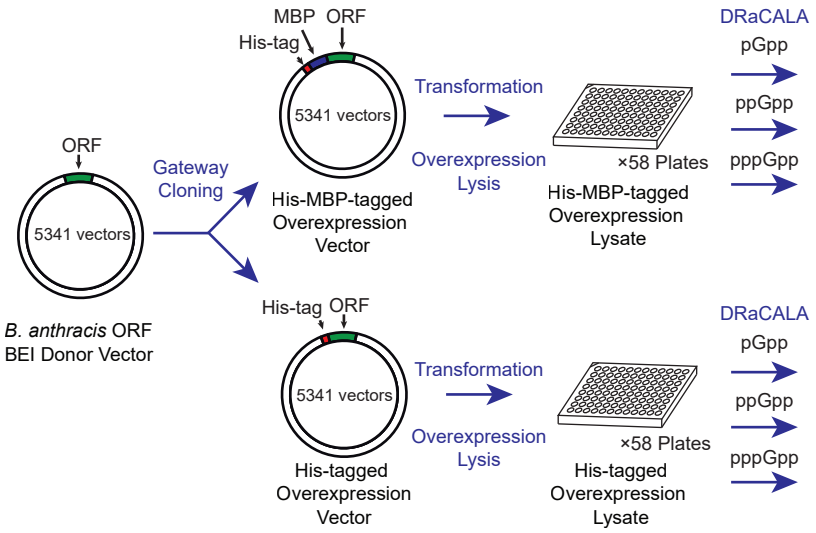


**b**

| Name | *B. anthracis* (This Work) | | | *E. coli* [19,20] | *S. aureus* [18] |
|---|---|---|---|---|---|
| | pppGpp | ppGpp | pGpp | (p)ppGpp | ppGpp |
| **Purine Synthesis Pathway** | | | | | |
| HprT | √ | √ | √ | √[19,20] | √ |
| Xpt | √ | √ | √ | NA | |
| Gmk | √ | √ | √ | | √ |
| PurA | √ | √ | √ | √[20] | |
| GuaC | Pending | √ | √ | | |
| PurR | √ | √ | √ | | |
| PurB | | | | √[20] | |
| PurC | | | | √[20] | |
| PurD | | | | √[20] | |
| PurF | | | | √[20] | |
| Gpt | NA | NA | NA | √[19,20] | |
| **Ribosome and Translation Regulation** | | | | | |
| HflX | √ | √ | | √[19] | √ |
| Der | √ | √ | | √[19,20] | |
| Obg | √ | √ | | √[19,20] | √ |
| RbgA | √ | √ | | NA | √ |
| TrmE | √ | √ | | √[19,20] | |
| Era | √ | √ | | √[19,20] | √ |
| **(p)ppGpp Metabolism** | | | | | |
| (p)ppGpp synthetase | √ | √ | √ | √[19] | |
| NuDiX hydrolase | √ | √ | | √(MutT)[19] | |
| 5′-nucleotidase | √ | √ | √ | √(UshA)[19] | |

**c**

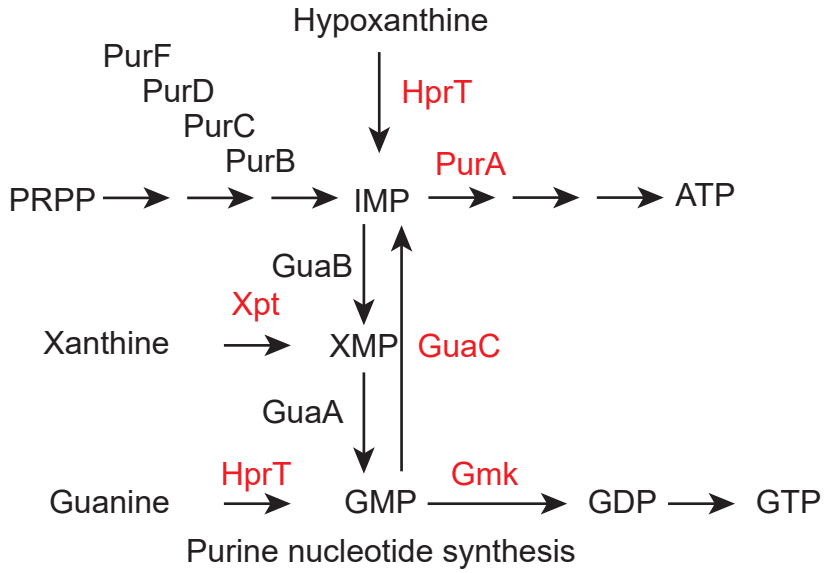


**d**

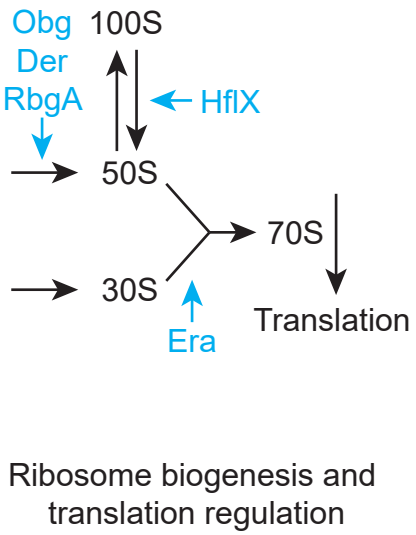


Red: bound by pGpp, ppGpp and pppGpp

Blue: bound by ppGpp and pppGpp, but not by pGpp

Fig. 2

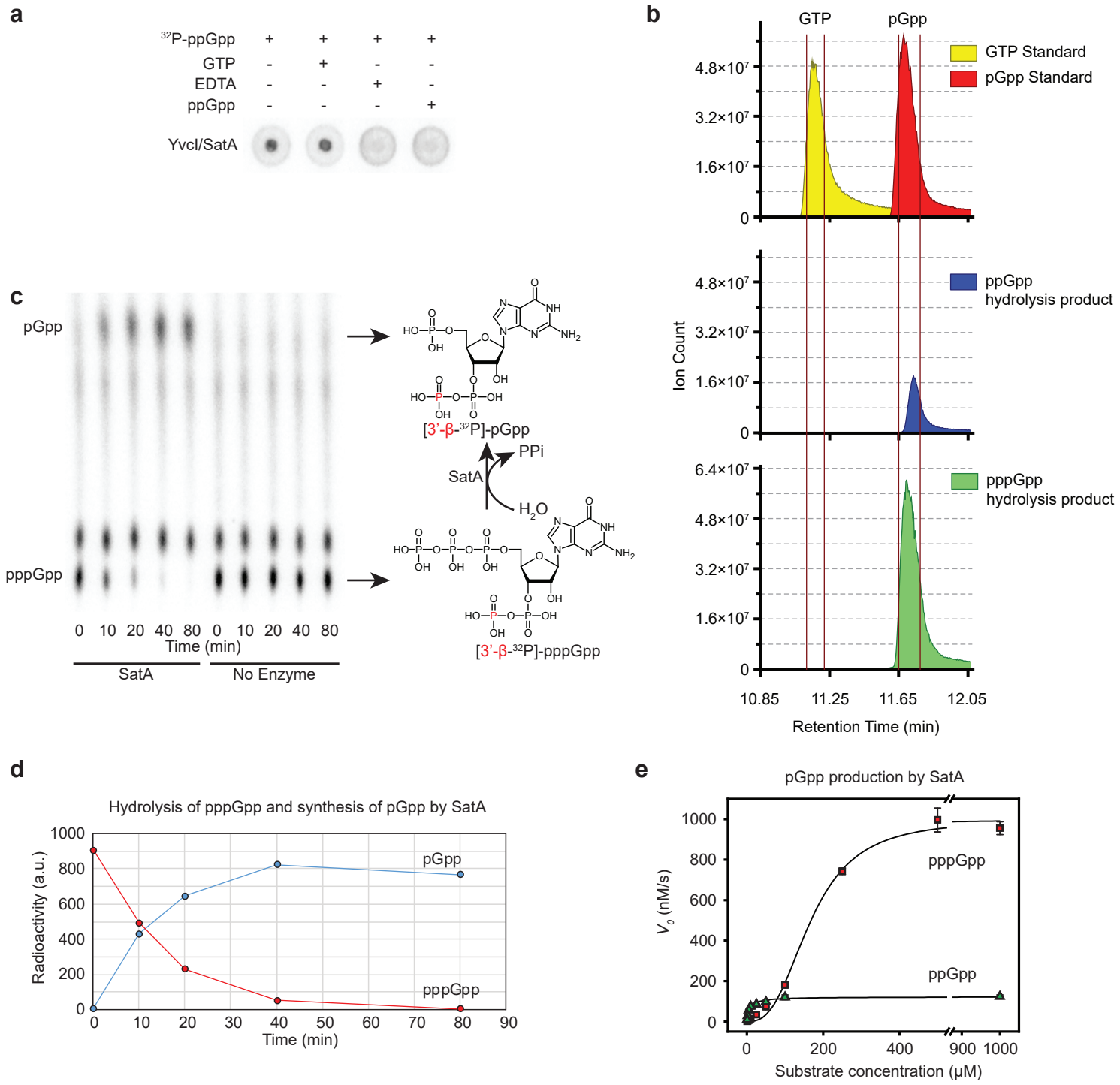
a
32P-ppGpp + + + +
GTP - + - -
EDTA - - + -
ppGpp - - - +
YvcI/SatA
b
GTP
pGpp
GTP Standard
pGpp Standard
ppGpp hydrolysis product
pppGpp hydrolysis product
Ion Count
4.8×10^7
3.2×10^7
1.6×10^7
0
6.4×10^7
10.85
11.25
11.65
12.05
Retention Time (min)
c
pGpp
pppGpp
0 10 20 40 80 0 10 20 40 80
Time (min)
SatA
No Enzyme
[3'-β-32P]-pGpp
PPi
SatA
H2O
[3'-β-32P]-pppGpp
d
Hydrolysis of pppGpp and synthesis of pGpp by SatA
Radioactivity (a.u.)
1000
800
600
400
200
0
pGpp
pppGpp
0 10 20 30 40 50 60 70 80 90
Time (min)
e
pGpp production by SatA
V0 (nM/s)
1000
800
600
400
200
0
pppGpp
ppGpp
0 200 400 900 1000
Substrate concentration (μM)

Fig. 3

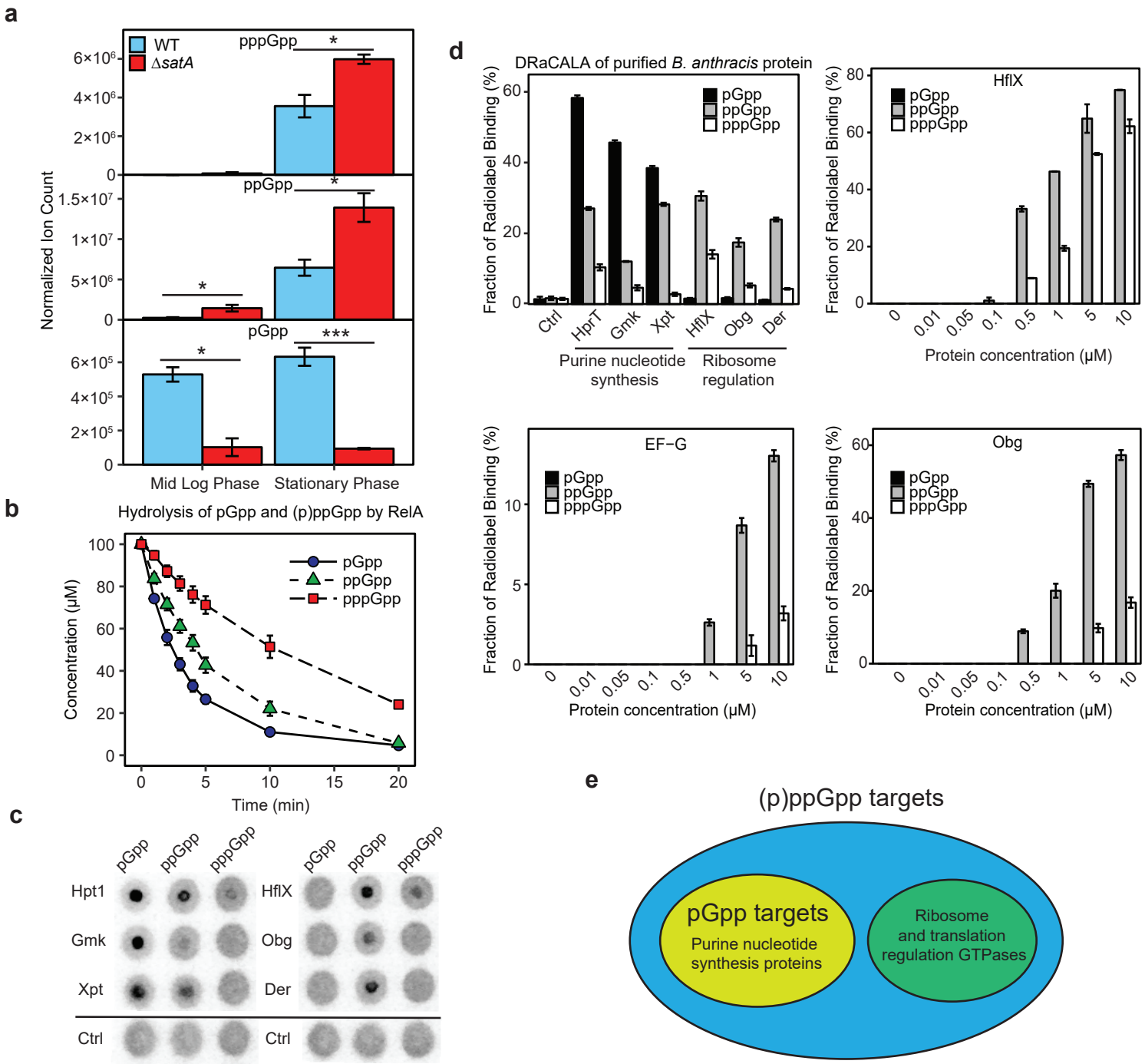
a
WT
ΔsatA
pppGpp
ppGpp
pGpp
Normalized Ion Count
Mid Log Phase
Stationary Phase
b
Hydrolysis of pGpp and (p)ppGpp by RelA
pGpp
ppGpp
pppGpp
Concentration (μM)
Time (min)
c
pGpp
ppGpp
pppGpp
Hpt1
Gmk
Xpt
Ctrl
HflX
Obg
Der
d
DRaCALA of purified B. anthracis protein
Fraction of Radiolabel Binding (%)
Ctrl
HprT
Gmk
Xpt
HflX
Obg
Der
Purine nucleotide synthesis
Ribosome regulation
Protein concentration (μM)
EF-G
e
(p)ppGpp targets
pGpp targets
Purine nucleotide synthesis proteins
Ribosome and translation regulation GTPases

Fig. 4

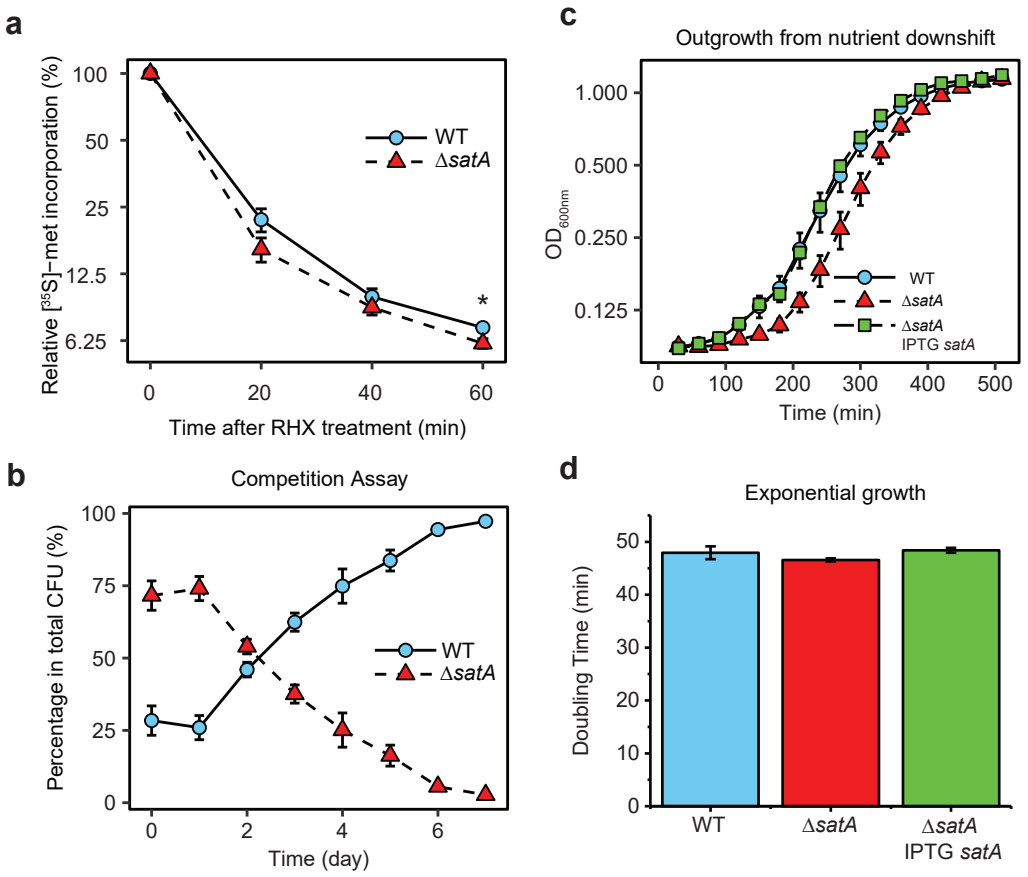
a
Relative [35S]–met incorporation (%)
100
50
25
12.5
6.25
WT
ΔsatA
*
0
20
40
60
Time after RHX treatment (min)
b
Competition Assay
Percentage in total CFU (%)
100
75
50
25
0
WT
ΔsatA
0
2
4
6
Time (day)
c
Outgrowth from nutrient downshift
OD600nm
1.000
0.500
0.250
0.125
WT
ΔsatA
ΔsatA
IPTG satA
0
100
200
300
400
500
Time (min)
d
Exponential growth
Doubling Time (min)
50
40
30
20
10
0
WT
ΔsatA
ΔsatA
IPTG satA

Fig. S1

```
1 Bsub_SatA            1 MTYLQRVTNCVLQTDDKVLLLQKP----RRGWWVAPGGKMESGESVRDSVIREYREETGIYIINPQLKGVFTFIIKD-GDHIVSEWMMFT 85
2 Ban_YvcI(BA5385)     1 ---MQRVTNCVLIRDNEVLLLQKP----RRNWWVAPGGKMERGETVRDSVVREYREETGIYLKNPALKGVFTFVIQE-GDKVVSEWMMFS 82
3 Bhalo_YvcI(BH3570)   1 ---MQRVTNCIVVDHDQVLLLQKP----RRGWWVAPGGKMEAGESILETVKREYWEETGITVKNPELKGIFSMVIFD-EGKIVSEWMLFT 82
4 EcMutT               1 MKKLQIAVGIIRNENNEIFITRRAADAHMANKLEFPGGKIEMGETPEQAVVRELQEEVGITPQHFSLFEKLEYEFPDRHITLWFWLVERW 90
5 EcNudG               1 MK-MIEVVAAIIERDGKILLAQRPAQSDQAGLWEFAGGKVEPDESQRQALVRELREELGIEATVGEYVASHQREVSGRIIHLHAWHVPDF 89
```

NuDIX Box

```
1 Bsub_SatA           86 FVADSYTGQNV-SESEEGKLQWHDVNDIQNLPMAPGDGHILDFMMKGQGLLHGTFTYTPEFELLSYRLDPQ-HIK--- 158
2 Ban_YvcI(BA5385)    83 FLATDFAGENK-LESEEGIIGWHTFDKIDDLAMAPGDYHIIDYLIKGNGIIYGTFVYTPDFELLSYRLDPS------- 152
3 Bhalo_YvcI(BH3570)  83 FKATEHEGEML-KQSPEGKLEWKKKDEVLELPMAAGDKWIFKHVLHSDRLLYGTFHYTPDFELLSYRLDPEPQMKKGV 159
4 EcMutT              91 EGEPWGKEGQP------GEWMSLVGLNADDFP--PANEPVIAKLKR----------------L--------------- 129
5 EcNudG              90 HGTLQAHEHQA------LVWCS--PEEALQYPLAPADIPLLEAFMA----------------LRAAR--PAD------ 135
```

Fig. S2

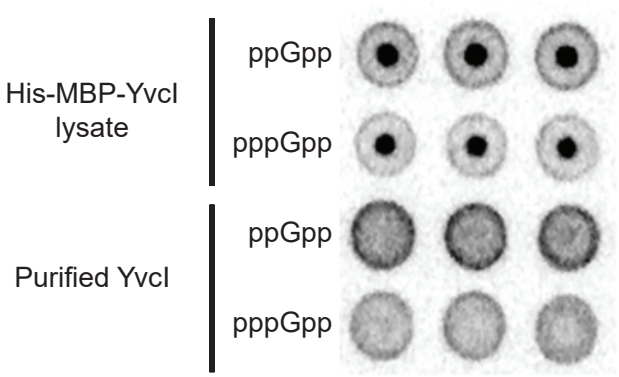
His-MBP-YvcI
lysate
ppGpp
pppGpp
Purified YvcI
ppGpp
pppGpp

Fig. S3

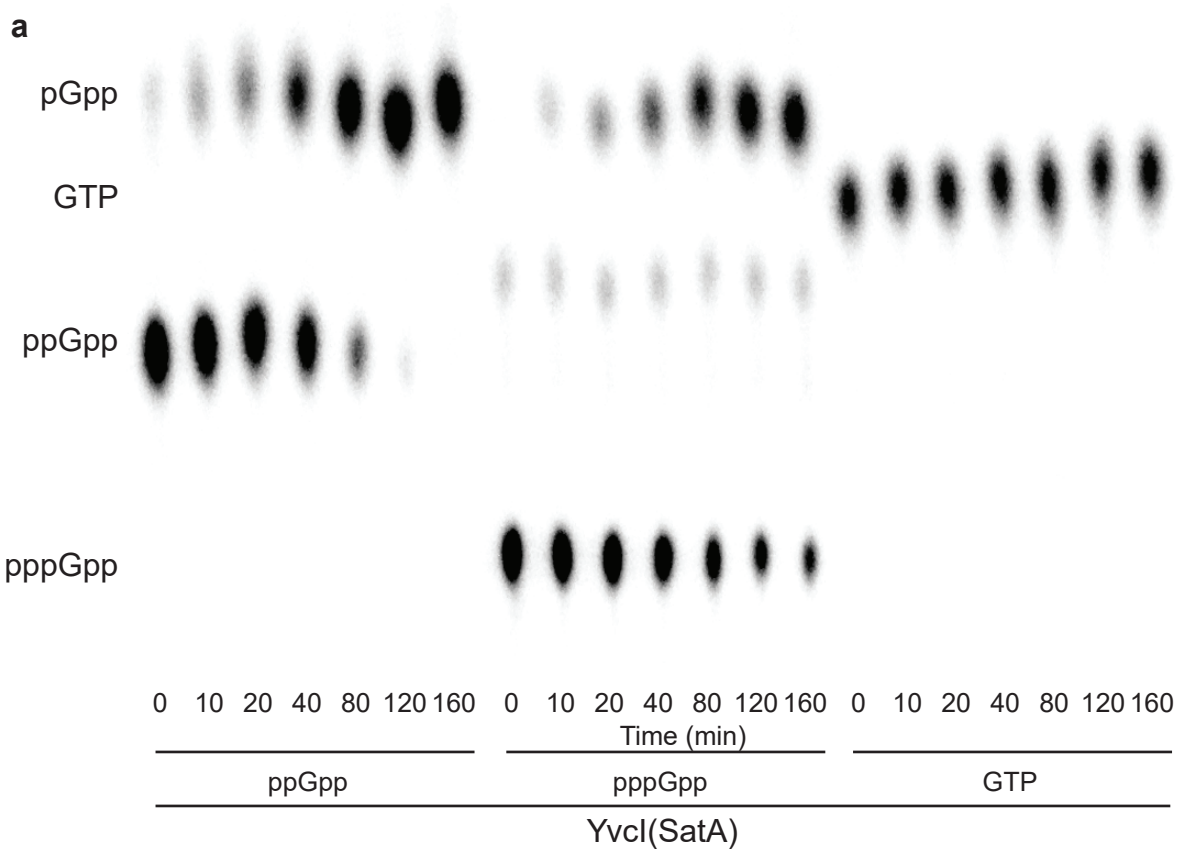
a
pGpp
GTP
ppGpp
pppGpp
0 10 20 40 80 120 160
0 10 20 40 80 120 160
0 10 20 40 80 120 160
Time (min)
ppGpp
pppGpp
GTP
YvcI(SatA)

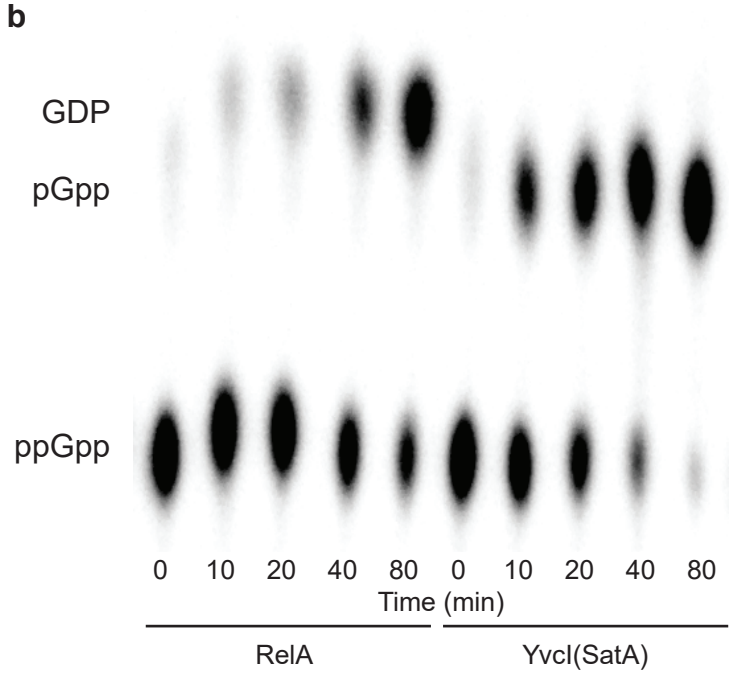
b
GDP
pGpp
ppGpp
0 10 20 40 80
0 10 20 40 80
Time (min)
RelA
YvcI(SatA)

Fig. S4

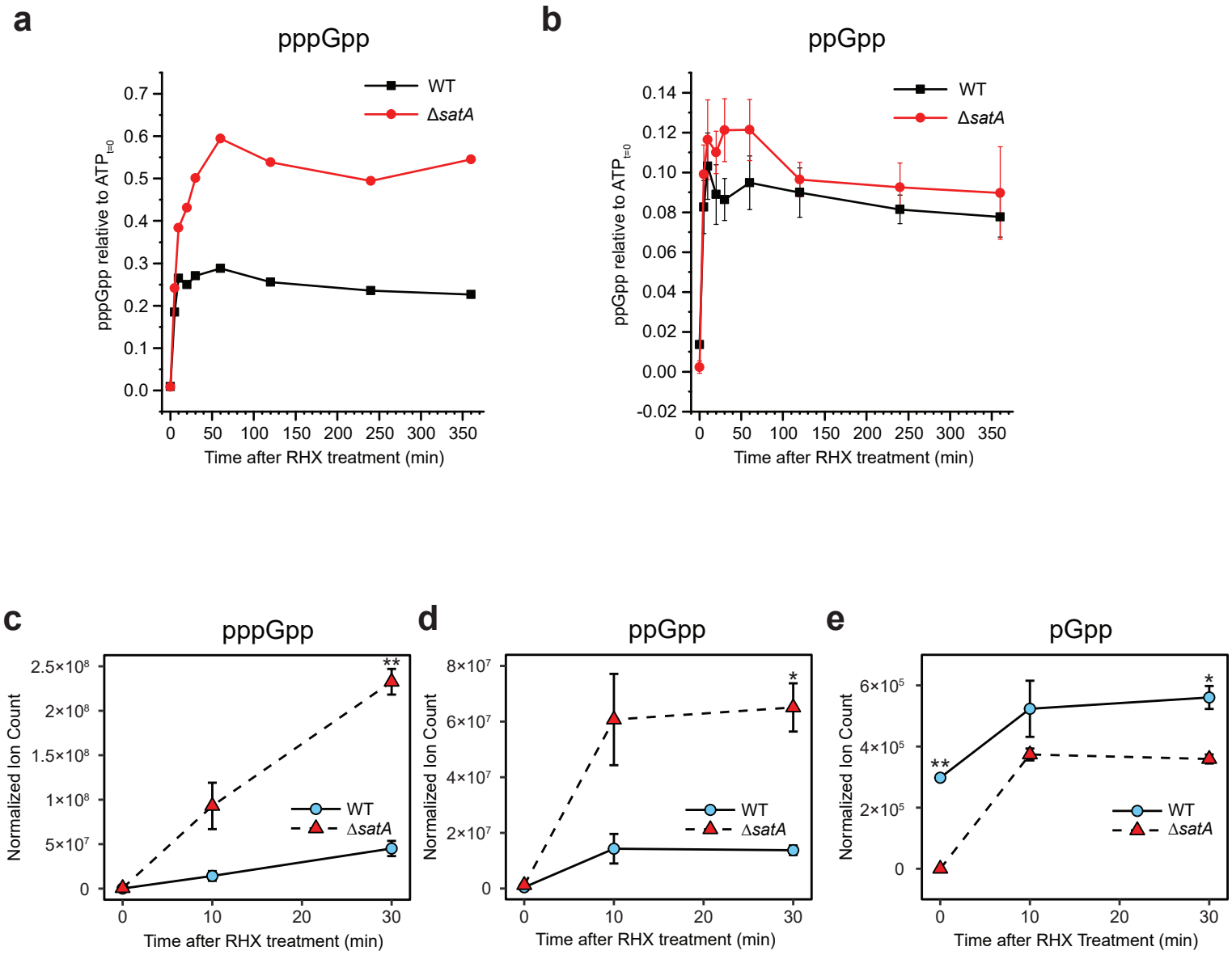
a
pppGpp
WT
ΔsatA
pppGpp relative to ATP$_{t=0}$
Time after RHX treatment (min)
b
ppGpp
WT
ΔsatA
ppGpp relative to ATP$_{t=0}$
Time after RHX treatment (min)
c
pppGpp
Normalized Ion Count
WT
ΔsatA
Time after RHX treatment (min)
d
ppGpp
Normalized Ion Count
WT
ΔsatA
Time after RHX treatment (min)
e
pGpp
Normalized Ion Count
WT
ΔsatA
Time after RHX Treatment (min)

Fig. S5

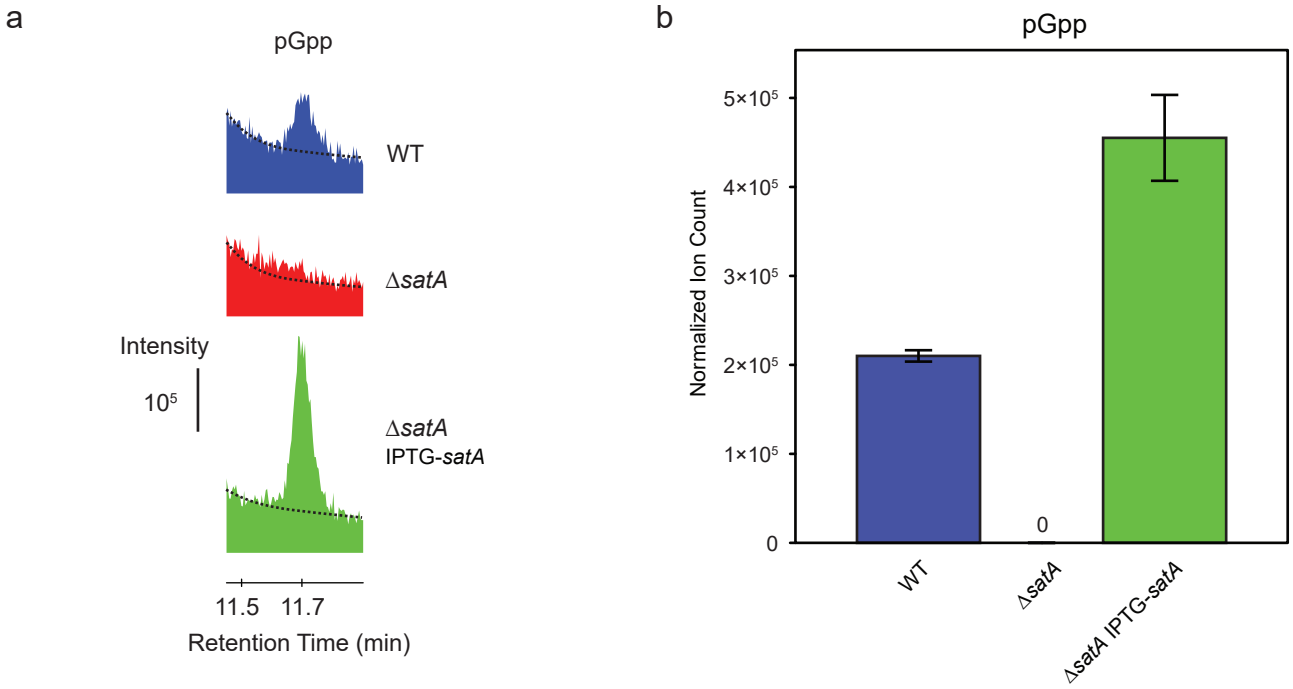
a
pGpp
WT
ΔsatA
Intensity
10⁵
ΔsatA
IPTG-satA
11.5
11.7
Retention Time (min)
b
pGpp
Normalized Ion Count
5×10⁵
4×10⁵
3×10⁵
2×10⁵
1×10⁵
0
0
WT
ΔsatA
ΔsatA IPTG-satA